

Elastic Scattering of 188-Mev Electrons from the Proton and the Alpha Particle*†‡§||¶

R. W. McALLISTER AND R. HOFSTADTER

Department of Physics and High-Energy Physics Laboratory, Stanford University, Stanford, California

(Received January 25, 1956)

The elastic scattering of 188-Mev electrons from gaseous targets of hydrogen and helium has been studied. Elastic profiles have been obtained at laboratory angles between 35° and 138° . The areas under such curves, within energy limits of ± 1.5 Mev of the peak, have been measured and the results plotted against angle. In the case of hydrogen, a comparison has been made with the theoretical predictions of the Mott formula for elastic scattering and also with a modified Mott formula (due to Rosenbluth) taking into account both the anomalous magnetic moment of the proton and a finite size effect. The comparison shows that a finite size of the proton will account for the results and the present experiment fixes this size. The root-mean-square radii of charge and magnetic moment are each $(0.74 \pm 0.24) \times 10^{-13}$ cm. In obtaining these results it is assumed that the usual laws of electromagnetic interaction and the Coulomb law are valid at distances less than 10^{-13} cm and that the charge and moment radii are equal. In helium, large effects of the finite size of the alpha-particle are observed and the rms radius of the alpha particle is found to be $(1.6 \pm 0.1) \times 10^{-13}$ cm.

I. INTRODUCTION

IN principle, it is possible to discover the finite size and structure of nuclei by methods of elastic electron scattering at high energies.¹⁻³ It is even possible to determine the structure of the proton by these methods.⁴ For the light nuclei the Born approximation is adequate to analyze the experimental data, while for heavier nuclei such as gold or even copper⁵ Yennie *et al.* have shown that a more accurate phase shift analysis is required.

The proton, deuteron, and alpha particle are most interesting to study because they are among the simplest nuclear structures. Furthermore, nuclei are built up out of protons and neutrons and it is fascinating to think of what the proton itself is built. In this paper we shall examine the structure of the proton and alpha particle. In an earlier paper⁶ the scattering from the deuteron was reported.

* The research reported in this document was supported jointly by the U. S. Navy (Office of Naval Research) and the U. S. Atomic Energy Commission, and by the U. S. Air Force through the Air Force Office of Scientific Research, Air Research and Development Command.

† Aided by a grant from the Research Corporation.

‡ These results were briefly reported at the Seattle Meeting of the American Physical Society, in July, 1954, but a comparison was not made at that time with the Rosenbluth results.

§ Miss Eva Wiener assisted in the early phases of this research. She was the victim of a fatal automobile accident in 1953.

|| Some of the material now reported was published earlier in brief form, *viz.*, R. Hofstadter and R. W. McAllister, *Phys. Rev.* **98**, 217 (1955).

¶ *Note added in proof.*—Results more recent than those reported in this paper and extending to 550 Mev, were presented at the New York meeting of the American Physical Society [Bull. Am. Phys. Soc. Ser. II, 1 (1956)] by Hofstadter, Chambers, and Blankenbender. The newer experiments confirm in greater detail the results presented in this paper. The newer results are being submitted for publication in *The Physical Review*.

¹ Hofstadter, Fechter, and McIntyre, *Phys. Rev.* **91**, 422 (1953).

² Hofstadter, Fechter, and McIntyre, *Phys. Rev.* **92**, 978 (1953).

³ Hofstadter, Hahn, Knudsen, and McIntyre, *Phys. Rev.* **95**, 512 (1954).

⁴ R. Hofstadter and R. W. McAllister, *Phys. Rev.* **98**, 217 (1955).

⁵ Yennie, Wilson, and Ravenhall, *Phys. Rev.* **92**, 1325 (1953).

⁶ J. A. McIntyre and R. Hofstadter, *Phys. Rev.* **98**, 158 (1954).

II. EXPERIMENTAL METHODS

Many of the experimental procedures have been reported in earlier papers.^{2,3} The only important new variation over earlier methods has been the substitution of a gaseous target for the previously used metallic foils. The gaseous target will now be described.

In Fig. 1, the basic design of the target assembly is given. The cylinder is made of 410 stainless steel and has been heat-treated to increase its strength. The end plates are made of 0.010-inch stainless steel and are deformed by the high-pressure gases into the approximate shape shown in the figure. The target cylinder is $3\frac{1}{8}$ inches long and $\frac{3}{4}$ inch in diameter. The end plates are sealed by means of O-rings shown in the figure. Pressures as high as 2000 pounds per square inch have been used successfully in this chamber over long periods of time.

The geometry of the scattering experiment using the gaseous target chamber is shown in Fig. 2. Because of the double-focusing characteristic of the magnetic spectrometer and because of the defining slits at the entrance and exit of the spectrometer, the effective target viewed by the spectrometer has the appearance indicated schematically in Fig. 2. It is evident that to a very good approximation the scattering yield at any given angle will be proportional to the cosecant of the angle of observation in the laboratory system since the

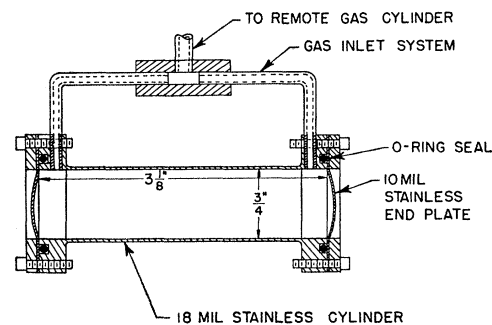


FIG. 1. Basic design of the gas chamber.

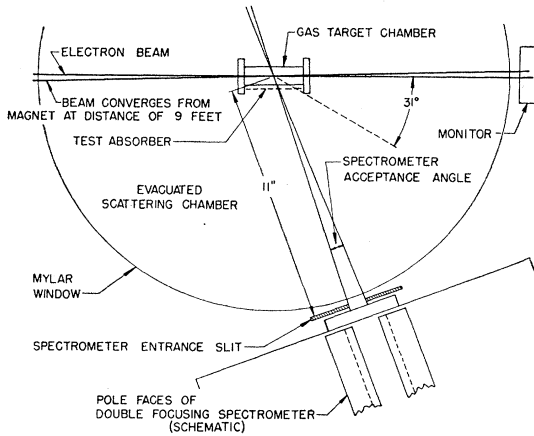


FIG. 2. Arrangement of parts in experiments on electron scattering from a gas target.

target thickness viewed by the spectrometer is proportional to this trigonometric function. Thus, to normalize the data to the same target thickness, the yield at any angle must be divided by the cosecant of the angle. In these experiments the effective target width viewed by the spectrometer is approximately $\frac{1}{2}$ inch at the gas chamber and this dimension is given by the vertical exit slit width (0.5 inch) imaged at the source.

The slit defining the acceptance angle in the plane common to the beam, scattering target, and entrance to the spectrometer, was $\frac{3}{4}$ inch wide and is indicated in Fig. 2. The exit collimator at the top of the magnet had a horizontal slit $\frac{5}{8}$ inch wide defining the energy band accepted by the Čerenkov detector, and a vertical slit $\frac{1}{2}$ inch wide. The vertical slit, together with the $\frac{3}{4}$ inch entrance slit, served to define the effective width of the target. In all the experiments herewith reported the incident beam was monochromatic within ± 1.0 Mev in 187 Mev.

At small angles, that is, angles less than 30° , it is possible for the spectrometer to view the end walls of the chamber and thus accept spurious electrons scattered by the target end plates. At 35° and 40° , a small residual effect of this type is present and is always subtracted from the yield furnished by the gas plus the target chamber. In other words, the scattering intensity is measured first with the gas in the chamber and then again with the gas removed from the target. The latter measurement gives the "background" due to the end wall effects. At all other angles, this effect is negligible.

Multiple scattering and radiation straggling from the 0.018-inch cylinder walls introduce only minor errors at the angles studied. This has been determined empirically by inserting a 0.010-inch stainless steel test absorber in the position so marked in Fig. 2. The test absorber was placed in the path of electrons scattered at angles 50° , 90° , and 130° . Elastic profiles were measured with the test absorber in and out of the path.

The peak of the elastic scattering profile was reduced 1 percent per mil of stainless steel in the direction of the scattered electrons, but the half-width of the curve was also increased by an amount such that the area under the elastic curve was the same, within 5 percent, whether the test absorber was in or out. This behavior may be understood as follows: The double focusing action of the spectrometer assures collection of all the electrons directed into the effective solid angle of the spectrometer, whether multiply-scattered or not and brings them to a focus beyond the energy slit (and from there into the Čerenkov detector). The only effects of multiple-scattering in the chamber walls are (a) to fuzz out the source of the scattered electrons in the gas, i.e., to increase or decrease the depth from which the scattered electrons appear to emerge from the target, (b) to reduce the angular resolution, and (c) to mix electrons scattered originally at different angles. Effect (a) may easily be seen to be of negligible importance. Effect (b) amounts to approximately $(\Delta\theta)_{\text{rms}} = \pm 1^\circ$. Since the angular opening of the lower spectrometer slit is $\pm 2^\circ$ and the multiple scattering is essentially Gaussian, the uncertainty in measuring the scattering angle is not appreciably increased by the effect of the side walls. The incoming end plate also contributes an uncertainty of $(\Delta\theta)_{\text{rms}} = \pm 0.7^\circ$. The resulting uncertainty, combining all causes, is approximately $(\Delta\theta)_{\text{rms}} = \pm 2.4^\circ$. The effect of multiple scattering in the hydrogen or helium gas volumes is of the order of 0.1° and hence negligible. In case (c), the error so introduced is of the order of tenths of a percent and is here neglected. In fact, plural scatterings are eliminated because of the energy selection of the spectrometer.

Radiation straggling of the electrons coming out through the walls of the chamber may be shown theoretically to contribute not more than a 5 percent relative correction between 50° and 90° and an equal figure between 90° and 130° , i.e., both the 50° yield and the 130° yield would each be lowered by something less than 5 percent with respect to the 90° yield. Our experiments with the test absorber have not demonstrated a consistent loss greater than 5 percent which could be attributed to straggling in the chamber walls. The statistical accuracy and drifts of the apparatus could have concealed an error of the order of 5 percent. Hence, we have not made a correction for straggling.

The lining-up procedure used a CsBr(Tl) crystal which could be moved remotely into or out of the beam. The crystal was placed along the beam axis just outside the scattering chamber. When it was desired to know the position of the beam, the crystal was moved into the beam and observed with a telescope. When the beam was lined up, say within $\pm \frac{1}{16}$ inch at the target, the crystal was withdrawn. Periodic checks showed whether or not the beam had moved. Very little beam motion was observed after an initial alignment.

An ion chamber was used in the early runs as a monitor of the incident beam, and a secondary electron

emitter⁷ in the later runs. The ion chamber showed a small amount of saturation at large beams and its runs were corrected by the empirically determined calibration of ion chamber *versus* secondary electron emitter. No correction so obtained was larger than 10 percent. If the correction had not been included, the proton size (see below) would have been a trifle larger.

The theoretical Schwinger radiation correction has not been applied since its angular dependence is very weak and well within the statistics of our experimental observations.

III. RESULTS

A. Hydrogen

Typical elastic profiles observed in a run with hydrogen at an incident energy of 185 Mev are shown in Fig. 3. Because of recoil of the struck proton the energy of the elastically deflected electron is a decreasing function of the angle of scattering. This may be observed by noting the variable position of the peaks in Fig. 3. Figure 4 shows the theoretical behavior of the energy of the scattered electron plotted against laboratory scattering angle for an incident energy of 187 Mev. The solid points show the positions of the peaks of the elastic scattering curves taken at the various angular positions during an experimental run at 187 Mev. The agreement is excellent except at extreme angles where small deviations are observed. The deviations are actually expected because of an increasing energy loss in the wall as the angle of entry becomes more and more oblique. The observed reduction in energy of the scattered electrons below the theoretical curve is in good agreement with the energy loss in the wall.

Because of the variation in energy of the scattered electrons we have been concerned that the solid angle effective in collecting electrons could have been smaller at small angles (high energies), where magnet saturation is important, than at large angles (smaller energies), where saturation is less important. To test this possibility we have measured the number of scattered electrons as a function of the entrance slit width at both

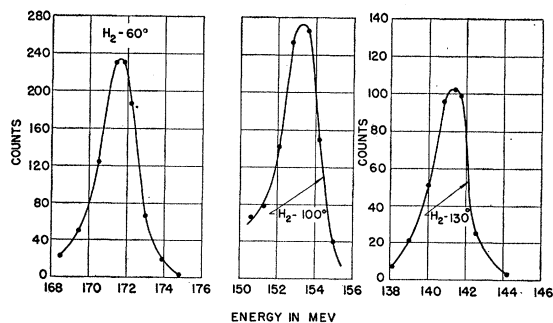


FIG. 3. Typical elastic profiles obtained with hydrogen gas at 185 Mev.

⁷ G. W. Tautfest and H. R. Fechter, Phys. Rev. **96**, 35 (1954); Rev. Sci. Instr. **26**, 229 (1955).

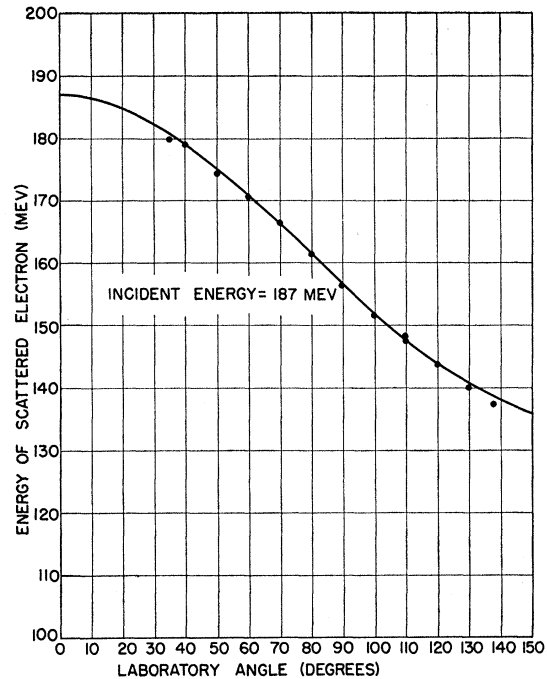


FIG. 4. The solid line gives the theoretical energy of the scattered electrons for an incident energy of 187 Mev. Relativistic kinematics are used to obtain the theoretical curve. The experimental points correspond to peak values of the elastic profiles and refer to experimental observations.

high (188 Mev) and low (139 Mev) energies. We have found that in both cases the number of scattered electrons for the $\frac{3}{4}$ -inch entrance slit width is 15 percent below the number expected from the initial slope of the curve of number of scattered electrons *versus* slit width. The 15 percent reduction is due to the widest trajectories striking the magnet chamber walls. In the radial direction in the magnet no electrons are lost because of the small extent of the beam in this direction. In other words, the effective solid angle is the same at both low and high energies provided that the entrance slit width is not larger than $\frac{3}{4}$ inch. Hence correction for magnet saturation is not required.

Areas under the elastic peaks, such as those of Fig. 3, have been measured by numerical integration over a width of ± 1.5 Mev about the peak. Such values have been plotted against laboratory angle as in Fig. 5. Areas over ± 2 and ± 2.5 Mev widths have also been obtained by numerical integration, but the relative results are essentially the same. Only the ± 1.5 Mev results will be presented below.

Figure 5 presents a summary of all the data obtained over a period of several months. It may be noticed that the experimental spread of points is somewhat larger than the statistical errors might lead one to expect. The causes of the spread are probably connected with small, unnoticed horizontal shifts of beam, hysteresis in the spectrometer magnet, small changes in the bias of the Cerenkov counter detection equipment, variations

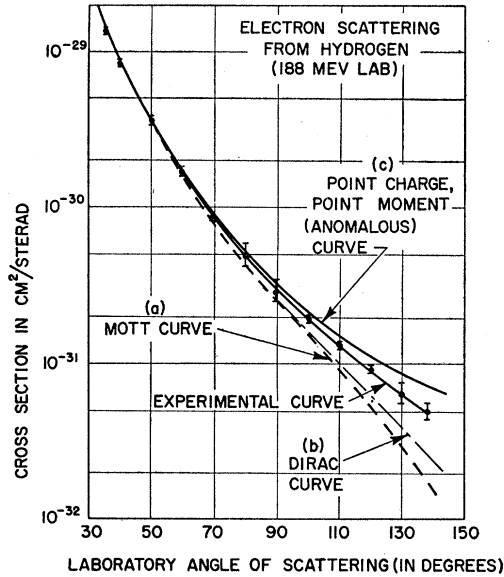


FIG. 5. Curve (a) shows the theoretical Mott curve for a spinless point proton. Curve (b) shows the theoretical curve for a point proton with the Dirac magnetic moment, curve (c) the theoretical curve for a point proton having the anomalous contribution in addition to the Dirac value of magnetic moment. The theoretical curves (b) and (c) are due to Rosenbluth.⁸ The experimental curve falls between curves (b) and (c). This deviation from the theoretical curves represents the effect of a form factor for the proton and indicates structure within the proton, or alternatively, a breakdown of the Coulomb law. The best fit indicates a size of 0.70×10^{-13} cm.

in saturation of the ion chamber monitor response and in the integrating voltmeter, and perhaps other unknown items. In Fig. 5 we have drawn a curve, labeled "experimental curve," which is our best estimate of the accumulated data at 188 Mev. The limits of error represent the greatest variations we have observed in any runs. However all runs, not being absolute, are normalized to each other by "best fitting." The experimental curve is also normalized to the theoretical curve at small angles. Also plotted in Fig. 5 are (a) the theoretical Mott curve for a spinless point proton, (b) the theoretical curve for a point proton with the Dirac value of magnetic moment (gyromagnetic ratio 2.00), (c) the theoretical curve for a point proton with the anomalous value of the proton moment in addition to the Dirac moment (gyromagnetic ratio = 5.58). The theoretical curves (b), (c) are obtained from calculations of Rosenbluth.⁸ The experimental curve deviates from curves (a), (b), and (c) at the larger angles and is lower than the curve for a point proton with anomalous moment, but higher than the curve for a point proton with Dirac moment. This reduction at large angles below the curve for point charge represents the effect of a "structure factor" or a "form factor" for the proton and hence indicates the finite size of the proton. Since the usual electromagnetic relations and the Coulomb

⁸ M. N. Rosenbluth, Phys. Rev. 79, 615 (1950).

interaction have been used in Rosenbluth's calculation, we are here assuming the validity of these interactions at small distances ($< 10^{-13}$ cm). Subject to this assumption, the experiment indicates the proton is not a point.

In order to carry out the form factor calculations, we have made use of Rosenbluth's formalism.⁸ However we have given the charge and magnetic moment phenomenological interpretations in place of the meson theoretic interpretations originally presented by Rosenbluth.⁹ We may write Rosenbluth's formulas as follows: for a point charge we have

$$\sigma = \sigma_{NS} \left\{ 1 + \frac{q^2}{4M^2} [2(1+\mu)^2 \tan^2(\theta/2) + \mu^2] \right\}, \quad (1)$$

where

$$\sigma_{NS} = \frac{e^4}{4E^2} \frac{\cos^2(\theta/2)}{\sin^4(\theta/2)} \frac{1}{1 + (2E/M) \sin^2(\theta/2)}, \quad (2)$$

and where

$$q = \frac{(2/\lambda) \sin(\theta/2)}{[1 + (2E/M) \sin^2(\theta/2)]^{1/2}}. \quad (3)$$

Here natural units, $\hbar = c = 1$, are used and the equations are written in terms of the laboratory coordinates; q is the invariant momentum transfer in the center-of-mass frame expressed in laboratory coordinates; E is the energy of the incident electrons; M the mass of the proton, and μ is the anomalous part of the proton's magnetic moment ($\mu = 1.79$). λ is the reduced de Broglie wavelength of the electron in the laboratory system.

For a diffuse proton we may write:

$$\sigma = \sigma_{NS} \left\{ F_1^2 + \frac{q^2}{4M^2} [2(F_1 + \mu F_2)^2 \tan^2(\theta/2) + \mu^2 F_2^2] \right\}, \quad (4)$$

where F_1 is the charge form factor (which also influences the intrinsic "Dirac" magnetic moment) and F_2 the anomalous magnetic moment form factor. In principle F_1 does not have to be the same as F_2 . F_1 and F_2 may be written as functions of $\langle q(r) \rangle$, where $\langle r \rangle$ is the root-mean-square radius of the appropriate charge, or moment distribution. F_1 and F_2 may also be identified with e'/e and $k'e'/k_0e$ in Rosenbluth's article.

We have not made detailed analyses for different F_1 and F_2 . Rather, as may be seen below, we have assumed $F_1 = F_2$. However, the data at all energies are quite consistent with this choice.

At the energies used in these experiments, the form factor (F_1 or F_2) is not appreciably shape dependent, i.e., one cannot distinguish between uniform, exponential, or Gaussian charge (or magnetic moment) distributions. All that can be determined is a mean square radius. Therefore we have tried to fit the experi-

⁹ We are indebted to Dr. D. R. Yennie for formulation of Eqs. (1)-(4).

mental data with a phenomenological form factor corresponding to various values of the mean square radii up to values of $q\langle r \rangle \cong 1.0$. q is again the momentum transfer and $\langle r \rangle$ the root-mean-square radius of the charge or magnetic moment distributions. For simplicity, as stated above, we have assumed that $\langle r \rangle_{\text{charge}} = \langle r \rangle_{\text{anomalous magnetic moment}}$, although in principle this is not a necessary restriction. Hence we can expect only to obtain a first approximation to the structure and size of the proton.

When such form factors are applied to the point charge-point moment curve, the behavior of the experimental curve can be reproduced very well. In fact for $\langle r \rangle_{\text{charge}} = \langle r \rangle_{\text{magnetic moment}} = 0.70 \times 10^{-13}$ cm the theoretical curve cannot be distinguished from the experimental curve within the limits of error. A separate theoretical curve for 0.70×10^{-13} cm therefore has not been included in Fig. 5. The limits of error in the radius are conservatively estimated at $\pm 0.24 \times 10^{-13}$ cm.

A similar fitting procedure can be employed with data obtained with electrons at 236 Mev in the incident beam. In this case our measurements could be made only at angles larger than or equal to 90° since our magnetic spectrometer cannot bend electrons of energy higher than those scattered at 90° (or smaller angles): For an incident energy of 236 Mev the scattered electron at 90° has an energy of 189 Mev, the approximate limit of our apparatus.

Figure 6 shows the experimental points obtained in several runs at 236 Mev. The shape of the point charge-point moment curve is shown as well as the experimental points. No absolute values are known for the experimental points so that the best that can be done is to try to fit the shape of the experimental curve with Eq. (4) for various values of F_1 and F_2 . Again the assumption $F_1 = F_2$ is made. Such attempts are shown in Fig. 6 and are labeled rms 6.2, 7.8, and 9.3×10^{-14} cm. The dotted curves corresponding to 6.2×10^{-14} cm and 9.3×10^{-14} cm may be shifted down or up respectively

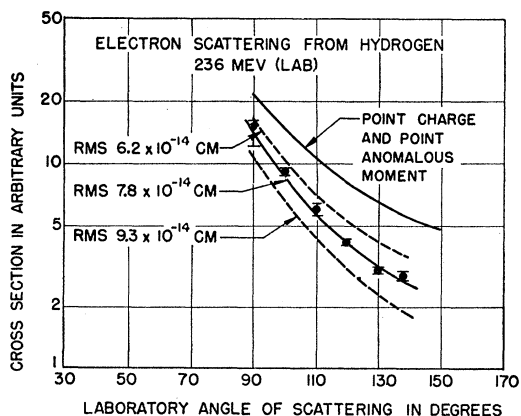


FIG. 6. This figure shows the experimental points at 236 Mev and the attempts to fit the shape of the experimental curve. The best fit lies near 0.78×10^{-13} cm.

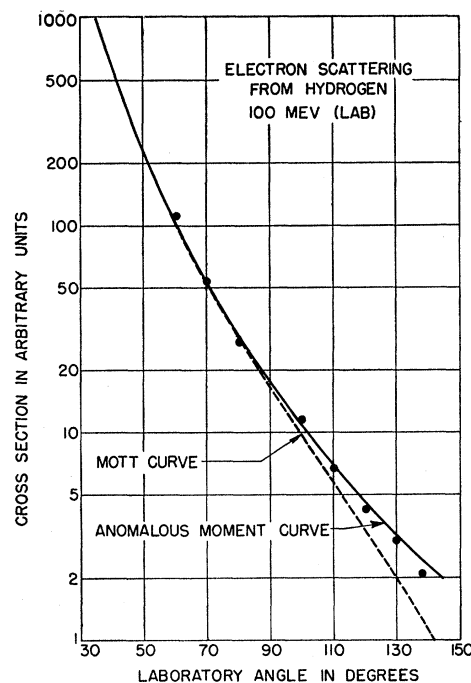


FIG. 7. Theoretical curves are shown for electrons of 100 Mev, along with the experimental observations at that energy.

to try to fit the experimental points, but neither curve will do so within the limits of error. Hence the data at 236 Mev support a "best" value of rms radius of $(0.78 \pm 0.20) \times 10^{-13}$ cm, conservatively speaking. This value is in good agreement with the best value $(0.70 \pm 0.24) \times 10^{-13}$ cm obtained above at 188 Mev.

In order to test some features of the apparatus, we have carried out a scattering experiment at an incident energy of 100 Mev. In this case, if our model of the proton is correct, the observed scattering should be quite close to the curve for a point charge and point moment because the $q\langle r \rangle$ value is small and $F^2 = 1.0$. Figure 7 shows that the agreement observed is highly satisfactory. At 100 Mev, the magnetic spectrometer is never saturated at any angle. Hence the "saturation" aspect and possible defocusing effects are not tested by this experiment. However, the 236-Mev and 188-Mev runs do test such possible effects since different energies correspond to different angular positions. The good agreement obtained between these latter two sets of data and the satisfactory behavior at 100 Mev is essentially what we have published earlier.⁴

These results may be summarized in the following way: If the proton can be assumed to (a) have distributions of charge and magnetic moment equal, or at least similar, in size and (b) if the Coulomb law and the usual electromagnetic laws are obeyed at distances of the order of 0.7×10^{-13} cm, then these experiments show that the proton has an rms radius of $(0.74 \pm 0.24) \times 10^{-13}$ cm. Of course, if the Coulomb law and the usual interactions are not valid, these findings could also be

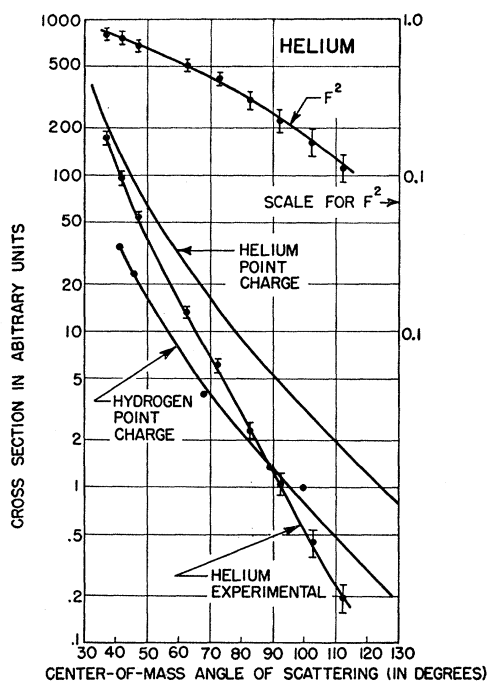


FIG. 8. The experimental curve for helium in the center-of-mass system, hydrogen normalizing points, and the helium point charge construction are shown. This figure also exhibits the square of the form factor as a function of angle. The best fit of theory to experiment corresponds to an rms radius of 1.60×10^{-13} cm.

interpreted in terms of a point charge and point moment. We suspect that the breakdown of the Coulomb law would have exhibited other consequences, possibly already recognized in the literature. Phenomenologically we cannot distinguish, at the present time with these experiments alone, between a finite size of the proton and a breakdown of the Coulomb law. Nevertheless, any meson theory would predict a finite size of the proton's magnetic moment and this is what we may have found in the proton.

B. Helium

The elastic peaks observed in helium are similar to those found in hydrogen, except that the recoil shifts are approximately four times smaller. To measure the form factor of the alpha particle with respect to electron scattering, we have made essentially simultaneous measurements of the scattering from helium and hydrogen and compared the results. The procedure involved carrying out the helium measurements, emptying the target chamber, and finally substitution of hydrogen for the helium. A series of measurements in

hydrogen is thus made almost at the same time as the helium measurements. From a few representative hydrogen points, we can construct a point-charge *Mott curve* for hydrogen, say, between 35° and 90° . If we multiply this curve by four ($Z_{\text{He}}^2 = 2^2 = 4$) we obtain a theoretical point-charge curve for helium. Note that we use a Mott curve (spinless particle) since the alpha particle has no spin or magnetic moment. The ratio of the actually observed experimental curve in helium to the point charge curve for helium gives the square of the form factor. Thus the form factor can be compared with theoretical form factors for various size charge distributions.

Figure 8 shows the helium experimental curve in the center-of-mass system, the hydrogen normalizing points, and the helium point-charge construction. The incident energy was 188 Mev for these experiments. Corrections for the different energies in the center-of-mass system and for the different effective solid angles have been made. A glance at the figure shows that the elastic scattering from the alpha particle is considerably smaller at large angles (a factor of 10 at 110°) than that from a point charge.

Figure 8 also shows the ratio of the alpha-particle scattering to that of a point charge with $Z=2$. This curve represents the square of the "form factor." The scale is given in the upper right hand corner of Fig. 8. This curve is indistinguishable from a (form factor)² curve for an rms radius of $(1.60 \pm 0.10) \times 10^{-13}$ cm. For such a small nucleus and an energy 188 Mev, our analysis will not give more than an rms radius from these measurements. It is curious that the rms radius of the alpha particle is approximately twice that of the proton as determined from these scattering measurements. Allowing for the rms radius of each of the two protons in the alpha particle, as determined above, the rms radius of the alpha particle would be smaller. By subtracting mean squares, the rms radius to the charge centroid would be 1.41×10^{-13} cm. This approximate calculation probably overemphasizes the effect of the finite protonic size.

ACKNOWLEDGMENTS

We wish to acknowledge the valuable cooperation of Mr. E. E. Chambers in helping with some of the measurements. We wish to thank Dr. R. H. Dalitz, Dr. D. G. Ravenhall, Dr. L. I. Schiff, and Dr. D. R. Yennie for many interesting conversations. We acknowledge with much appreciation the valued help of the late Miss Eva Wiener.